Region-specific regulation of stem cell-driven regeneration in tapeworms.

Tania Rozario[1*], Edward B. Quinn[1], Jianbin Wang[2], Richard E. Davis[2], and Phillip A. Newmark[1,3,4*]

[1]Morgridge Institute for Research, Madison, WI, USA, [2]Department of Biochemistry and Molecular Genetics, RNA Bioscience Initiative, University of Colorado School of Medicine, Aurora, CO, USA, [3] Howard Hughes Medical Institute, [4]Department of Integrative Biology, University of Wisconsin-Madison, Madison, WI, USA.

* corresponding authors

Email: pnewmark@morgridge.org

trozario@morgridge.org

Abstract

Tapeworms grow at rates rivaling the fastest-growing metazoan tissues. To propagate they shed large parts of their body; to replace these lost tissues they regenerate proglottids (segments) as part of normal homeostasis. Their remarkable growth and regeneration are fueled by adult somatic stem cells, that have yet to be characterized molecularly. Using the rat intestinal tapeworm, *Hymenolepis diminuta*, we find that regenerative potential is regionally limited to the neck, where head-dependent extrinsic signals create a permissive microenvironment for stem cell-driven regeneration. Using transcriptomic analyses and RNA interference, we characterize and functionally validate regulators of tapeworm growth and regeneration. We find no evidence that stem cells are restricted to the regeneration-competent neck. Instead, lethally irradiated tapeworms can be rescued when cells from either regeneration-competent or regeneration-incompetent regions are transplanted into the neck. Together, the head and neck tissues provide extrinsic cues that regulate stem cells, enabling region-specific regeneration in this parasite.

Introduction

Tapeworms are parasitic flatworms that infect humans and livestock, causing lost economic output, disease, and in rare cases, death[1]. These parasites are well known for their ability to reach enormous lengths. For example, humans infected with the broad or fish tapeworm, *Diphyllobothrium latum*, harbor parasites that average 6 m in length[2]. It is less commonly appreciated that tapeworms can regenerate to accommodate their multi-host life cycle. Adult tapeworms in their host intestines develop proglottids (segments) that are gravid with embryos. Tapeworms pinch off the posterior and gravid sections of their body, which exit with the host excrement, to be eaten by a suitable intermediate host that supports larval tapeworm development. Despite losing large body sections, the tapeworm does not progressively shorten; instead, it regenerates proglottids, allowing the worms to maintain an equilibrium length. Despite this remarkable biology, tapeworms are an unexplored animal model in the study of regenerative behaviors.

Up to the 1980s the rat intestinal tapeworm, *Hymenolepis diminuta*, had been a favorite model organism among parasitologists. *H. diminuta* grows rapidly–within the first 15 days of infection, it produces up to 2200 proglottids, increases in length by up to 3400 times, and weight by up to 1.8 million times [3]–and is easily propagated in the laboratory. Foundational work on their biochemistry, ultrastructure, and developmental biology enriched our understanding of these tapeworms[4]. However, with the dawn of the molecular age and the rise of genetic model organisms, *H. diminuta* was essentially left behind. Here, we show that *H. diminuta* is an excellent, tractable model for the study of stem cells and regeneration, with the power to inform us about parasite physiology.

As an obligate endoparasite, adult *H. diminuta* will expire once its host rat dies. However, the lifespan of *H. diminuta* can be greatly increased via regeneration. A single adult tapeworm can be serially amputated and transplanted into a new host intestine, where the fragment can regenerate into a mature tapeworm even after 13 rounds of amputation over 14 years[5]. These observations have led to speculation that *H. diminuta* may be inherently immortal. This situation is reminiscent of the free-living cousins of tapeworms: freshwater planarians like *Schmidtea mediterranea*, which reproduce indefinitely by fission, and can regenerate their whole body from tiny fragments.

Planarian immortality and regeneration are enabled by adult somatic stem cells called neoblasts[6-8]. These stem cells are the only dividing undifferentiated cells within the soma. Like planarians, *H. diminuta* maintains a population of neoblast-like adult somatic stem cells[3] that are likely responsible for their growth and regenerative ability. Recently, stem cells of multiple species of parasitic flatworms have been described[9-13]. Stem cells play crucial roles in parasite development, transmission, homeostasis, and even disease. For example, stem cells enable prolific reproduction and longevity[14], mediate host-parasite interactions[15], and allow metastatic parasite transmission in host tissues[16]. How stem cells may regulate regeneration in parasites such as tapeworms is largely unexplored and the subject of this study.

We use *H. diminuta,* to investigate the molecular basis of tapeworm regeneration. We have established and refined experimental tools such as transcriptomics, *in vitro* parasite culture, whole-mount and fluorescent RNA *in situ* hybridization (WISH and FISH), cycling-cell tracing with thymidine analogs, RNA interference (RNAi), and cell transplantation, all described in this work. We determine that the ability to regenerate is regionally limited to the neck of adult *H. diminuta*. However, regeneration from the neck is finite without signals from the tapeworm head. Using RNA sequencing (RNA-seq), we identify and characterize various markers of the somatic

cycling-cell population, which includes tapeworm stem cells. Using RNAi, we functionally validate molecular regulators of growth and regeneration. However, our analyses failed to uncover a neck-specific stem cell population that explains the regional regenerative ability displayed by *H. diminuta.* Instead, we show that cells from both regeneration-competent and regeneration-incompetent regions of *H. diminuta* have stem cell ability and can restore viability to lethally irradiated tapeworms. Our results show that extrinsic signals present in the tapeworm neck, rather than specialized stem cells, confer region-specific regenerative ability in this tapeworm.

Results

The anatomy of adult *H. diminuta* consists of a head with four suckers, an unsegmented neck, and a body with thousands of proglottids/segments that grow and mature in an anterior-to-posterior direction[3,17] (Fig. 1a). What regions of the tapeworm body are competent to regenerate? In order to test regeneration competency, it is necessary to grow tapeworms *in vitro* instead of in the intestine, where the suckers are required to maintain parasites *in vivo*. We established *H. diminuta in vitro* culture conditions modified from Schiller's method[18] and tested the regeneration competence of 1 cm amputated fragments (Fig. 1b-c). The anterior-most fragments (head+neck+body) were competent to regenerate, confirming *in vivo* observations using amputation and transplantation[5,19]. Anterior fragments that were first decapitated (neck+body) were also competent to regenerate. In contrast, "body only" fragments failed to regenerate proglottids. All amputated fragments could grow in length (Fig. 1d), differentiate mature reproductive structures, and mate. However, the neck is necessary for regeneration of new proglottids over time. In no case did we observe head regeneration. Furthermore, amputated heads alone could not regenerate *in vitro* (data not shown) nor *in vivo*[5]. The neck is also sufficient for proglottid regeneration as 2 mm "neck only" fragments regenerated an average of 383 proglottids (SD=138, N=4, n=20) after 12 days *in vitro* (Fig. 1e).

Previous *in vivo* studies have shown that *H. diminuta* can regenerate after serial rounds of amputation and transplantation for over a decade[5] and perhaps indefinitely. Using *in vitro* culture, we confirmed that anterior fragments of *H. diminuta* can regenerate after at least four rounds of serial amputation (Fig. 1f-g). Decapitated (-head) fragments regenerated proglottids after the first amputation; however, re-amputation abrogated regeneration (Fig. 1f-g). After decapitation, a definitive neck could not be maintained and eventually, the whole tissue was comprised of

proglottids (Fig. 1–figure supplement 1). Without the head, proglottid regeneration from the neck is finite. Thus, while the neck is both necessary and sufficient for proglottid regeneration, the head is required to maintain an unsegmented neck and for persistent regeneration.

If signals from the head regulate regeneration, is regenerative potential asymmetric across the anterior-posterior (A-P) axis of the neck? We subdivided the neck into three 1 mm fragments and found that the most-anterior neck fragments regenerated more proglottids than the middle or posterior neck fragments (Fig. 1h-i). Thus, regeneration potential is asymmetric across the neck A-P axis with a strong anterior bias.

Since the neck is the only region competent to regenerate, are stem cells preferentially confined to the neck? In lieu of specific molecular markers for stem cells, we examined the distribution of all cycling cells in adult tapeworms. In *H. diminuta,* the only proliferative somatic cells are undifferentiated[20,21], thus, cycling somatic cells include tapeworm stem cells and any dividing progeny. To label cycling cells, we used two methods: uptake of the thymidine analog F-*ara*-EdU[22] to mark cells in S-phase and FISH against cell cycle-regulated transcripts, such as the replication licensing factor *minichromosome maintenance complex component 2* (*mcm2*) and *histone h2b* (*h2b*), which are conserved stem cell markers in free-living and parasitic flatworms[9,23]. We detected cycling somatic cells throughout the tapeworm body (Fig. 2a-b). Contrary to previous results[20], we also detected cycling cells in the head, though in small numbers (Fig. 2a). The scarcity of these cells may be the reason they were originally missed. Taken together, cycling cells are present in all regions, regardless of regeneration competence.

To further our understanding of how tapeworm stem cells are distributed and regulated, we sought to identify stem cell markers. Stem cell genes have been discovered previously in flatworms by identifying transcripts downregulated after exposure to irradiation, which depletes cycling

cells[9,23,24]. Exposing *H. diminuta* to 200 Gy X-irradiation reduced the number of cycling cells by 91±6% after 3 days (Fig. 2c-d) and caused stunted growth and regeneration (Fig. 2–figure supplement 1). We leveraged the sensitivity of *H. diminuta* to irradiation in order to identify new molecular markers of cycling somatic cells by RNA-seq (Fig. 2e). A *de novo* transcriptome of 14,346 transcripts was assembled (see Materials and Methods) to which sequencing reads were mapped. We identified 683 transcripts that were irradiation sensitive (downregulated; FDR ≤0.05) (Supplemental Table 1). Expression of irradiation-sensitive genes by WISH was indeed reduced after exposure to irradiation, validating our RNA-seq approach (Fig. 2–figure supplement 2).

Two rounds of expression screening were then applied to hone in on cycling-cell genes from our irradiation-sensitive dataset (Fig. 2e). The position of cycling cells in the neck is spatially restricted in a conserved pattern[25] (Fig. 3a): cycling cells reside in the neck parenchyma bounded by the nerve cords and are absent from the animal edge where muscle and tegument (parasite skin) are located[20]. Among 194 irradiation-sensitive transcripts that displayed clear WISH patterns, 63% were expressed in the neck parenchyma, though in a variety of patterns (Fig. 3–figure supplement 1). 13% showed similar patterns to *h2b* and *mcm2* (Fig. 3b-c, Fig. 3–figure supplement 1b). These include the nucleic acid binding factor *Zn finger MYM type 3* (*zmym3)*, the transcription factor *suppressor of hairy wing* (*su(Hw)*), *NAB co-repressor domain 2 superfamily member* (*nab2*), and nuclear lamina component *laminB receptor* (*lbr*). 25% of irradiation-sensitive genes, were expressed in a minority of cells in the neck parenchyma (Fig. 3–figure supplement 1c). 24% were expressed within the parenchyma and more broadly toward the animal edge (Fig. 3–figure supplement 1d). The remainder represented genes expressed at segment boundaries or in differentiated tissues (Fig. 3–figure supplement 1e-f). In conclusion, irradiation-sensitive

transcripts identified by RNA-seq likely represent markers for stem cells, progenitors, and even differentiated cells that were lost or compromised following irradiation.

To focus on genes with enriched expression in cycling cells, we performed double FISH (dFISH) with candidate genes and either *h2b* or *mcm2,* which we used interchangeably as they are co-expressed in the neck parenchyma (Fig. 3–figure supplement 2). After dFISH for 53 candidates, 72% of genes tested were co-expressed in cycling cells (Fig. 3–figure supplement 3a, Supplemental Table 2). The irradiation-sensitive transcripts from Fig. 3c were indeed colocalized in cycling somatic cells (Fig. 3d). One gene, the homeobox factor *prospero* (*prox1*), was expressed exclusively in a subset of cycling cells (Fig. 3–figure supplement 3b). We confirmed that genes whose expression only partially overlapped in the neck parenchyma, such as the Zn finger-containing gene *HDt_10981* and *palmitoyl-protein thioesterase 1 (ppt1)*, were expressed in both cycling cells and non-cycling cells (Fig. 3–figure supplement 3c). We propose that these genes likely represent lineage-committed stem cells or progenitors for tissues such as muscle, neurons, tegument, or protonephridia. 28% of irradiation-sensitive genes were predominantly expressed in non-cycling cells that were juxtaposed to cycling cells (Fig. 3–figure supplement 3d). In summary, our analysis revealed a heterogeneous and complex mixture of cell types or states in the neck parenchyma as well as within the cycling-cell population.

What role(s) do the newly identified cycling-cell genes play during regeneration? We developed an RNAi protocol to knock down target genes, confirm knockdown by quantitative PCR (Fig. 4–figure supplement 1), and assay for defects in growth and regeneration (Fig. 4a). As a proof of principle, we knocked down *h2b,* which should compromise growth due to cycling-cell loss, as observed in other flatworms[15,23]. Knockdown of *h2b, zmym3,* and *su(Hw)* each resulted in diminished growth and regeneration (Fig. 4b-c). The number of proglottids regenerated was also

reduced, but could not be quantified as many RNAi worms were so thin and frail that proglottid definition was lost.

Are these RNAi-induced failures in growth and regeneration due to defects in the cycling-cell population? RNAi knockdown of *h2b, zmym3,* and *su(Hw)* severely reduced the number of cycling cells in the neck (Fig. 4d-e). The loss of F-*ara*-EdU uptake after RNAi could be due to a failure of proliferation or to loss of the cell population. Thus, we performed WISH to detect the cycling-cell marker *mcm2* and observed a reduction of this cell population after RNAi (Fig. 4f). Taken together, *h2b, zmym3,* and *su(Hw)* are necessary for the maintenance of the cycling-cell population, including stem cells, in *H. diminuta*.

Although we have identified heterogeneity within the cycling-cell population of the neck parenchyma and uncovered genes that are required for growth and regeneration, it remains unclear why regeneration competence is restricted to the neck. By WISH all cycling-cell genes, including *zmym3* and *su(Hw)*, were detected throughout the whole tapeworm body (Fig. 4g). Since we observed an anterior bias in regenerative ability (Fig. 1h-i), we hypothesized that RNA-seq may reveal an anteriorly biased stem cell distribution. Thus, we performed RNA-seq of 1 mm anterior, middle, and posterior neck fragments (Fig. 1h), and identified 461 anterior-enriched and 241 anterior-depleted transcripts (Supplemental Table 3). By WISH, anterior-enriched and anterior-depleted transcripts were often detected in corresponding gradients (Fig. 5a), but in patterns that were excluded from the neck parenchyma. When we overlaid the anterior-enriched and -depleted datasets with our irradiation-sensitive dataset, the majority of anterior-enriched transcripts (88%) were not irradiation sensitive (Fig. 5b). Our results suggest that the A-P polarized signals across the neck region arise predominantly within the non-cycling compartments.

Since our RNA-seq analysis identified 57 transcripts that were anterior enriched and irradiation sensitive, we examined expression patterns within this category. We found 15 genes expressed in a subset of cells within the neck parenchyma (Fig. 5c), but 7/8 genes tested were not expressed in cycling cells (Fig. 5d, Supplemental Table 2). Only one gene, *prox1,* was co-expressed in cycling cells (Fig. 3–figure supplement 3b). These analyses have not revealed an anteriorly biased subpopulation of stem cells that confer regenerative ability.

With no evidence for a unique neck-specific subpopulation of stem cells, we hypothesized that stem cells may be distributed throughout the tapeworm, but that extrinsic signals functioning in the neck are necessary to instruct stem cell behavior and/or proglottid regeneration. We designed a functional assay to test populations of cells for the ability to rescue regeneration, modelled after similar experiments performed on planarians[8]. We exposed tapeworms to a lethal dose of irradiation, injected cells from wild-type donors into the neck region, amputated 5 mm anterior fragments, and assayed rescue of lethality and regeneration after 30 days *in vitro*. Remarkably, bulk-cell transplants were able to either partially or fully rescue irradiated worms that were destined to die (Fig. 6a, c). “Full” rescue was ascribed to worms with normal adult appearance whereas “partial” rescue was assigned to cases in which proglottids were regenerated but the worms displayed abnormalities, like contracted necks (Fig. 6–figure supplement 1a). We did not observe any proglottid regeneration in irradiated worms with or without buffer injection (Fig. 6a, c).

Is the rescue ability described above dependent on tapeworm cycling cells? We exposed donors to F-*ara*-EdU for 1 hr, to label cycling cells prior to transplantation into irradiated hosts (Fig. 6–figure supplement 1b). Though bulk-cell transplants were performed, injection sites contained 0, 1, or small groups of F-ara-EdU^{+} cells immediately after transplantations (Fig. 6–

figure supplement 1c), likely due to technical challenges. Despite this issue, we were able to detect large colonies of F-ara-EdU^{+} cells 3 days post-transplantation (Fig. 6–figure supplement 1d). We also observed that some labeled cells were incorporated into terminally differentiated tissues at the animal edge (Fig. 6–figure supplement 1d: inset). Thus, cycling cells from donors are able to become established and differentiate inside the irradiated host.

To test if the cycling-cell population is necessary to rescue lethally irradiated tapeworms, we depleted cycling cells from donor worms using hydroxyurea (HU), which resulted in 96±3% loss of cycling cells after 6 days (Fig. 6–figure supplement 1e-f). Cycling cells are essential for rescue of regeneration as injected cells from HU-treated donors rescued only 1% of the time, compared to 24% rescue using cells sourced from sister donors that did not receive the drug (Fig. 6b-c). HU was used to deplete cycling cells instead of irradiation in order to avoid inducing DNA damage in the transplanted cells. Cells transplanted from HU-treated donors had otherwise comparable morphology to untreated cells (Fig. 6–figure supplement 1g). Our results suggest that tapeworm cycling cells contain *bona fide* stem cell activity.

With this functional assay in hand, we examined the rescue ability of cells from anterior donor tissues (including the regeneration-competent neck) compared to posterior donor tissues (which are regeneration incompetent). Cells from either region were able to rescue regeneration in lethally irradiated tapeworms (Fig. 6b-c). These results support the idea that the regeneration competence of the neck is due to extrinsic signals that regulate regeneration, rather than intrinsic properties of stem cells in the neck region. It appears that in tapeworms, location matters enormously: the head and neck environment provide cues that regulate the ability of stem cells to regenerate proglottids, even though cycling cells (and likely stem cells), are not anatomically confined.

Discussion

Across the flatworm phylum, both free-living and parasitic worms maintain stem cells throughout adulthood but display a range of regenerative abilities. The freshwater planarian *S. mediterranea* can regenerate its whole body from tiny amputated fragments. The blood fluke *Schistosoma mansoni* cannot regenerate after amputation, though it does employ adult somatic stem cells in other ways, such as to repair injury[26] and produce prodigious numbers of eggs[27]. Prior to this study, the regenerative ability of tapeworms had never been comprehensively tested. Although it was known that anterior fragments containing the head, neck, and immature proglottids could regenerate into fully mature tapeworms once transplanted into a rat intestine[5,19], fragments lacking heads could not be tested for regenerative ability using transplantation. Attempts were made to suture *H. diminuta* fragments with mutilated or removed heads into a rat intestine but these fragments were invariably flushed out[19]. Here we employ a robust *in vitro* culture system that allowed us to test regeneration of any amputated *H. diminuta* fragment for the first time. We show that the neck is both necessary and sufficient for proglottid regeneration, though this regenerative ability is ultimately finite without regulatory signals that depend on the presence of the head. *H. diminuta* is an intriguing model to discover signals that both drive and limit regenerative ability.

During homeostasis, the neck of *H. diminuta* serves as a "growth zone" from which proglottids are thought to bud one at a time[28], thus, it makes intuitive sense that this tissue would retain the ability to regenerate proglottids post-amputation. Furthermore, cells with the typical morphology of stem cells are resident in the neck[20]. However, we find that cycling cells are present in all regions regardless of regenerative competence. Thus, it was necessary to embark on a more

thorough characterization of tapeworm cycling cells to understand how *H. diminuta* may regulate stem cells and enable proglottid regeneration.

Adult somatic stem cells in free-living flatworms have already been well described molecularly, and share many conserved regulators. However, parasitic flatworms have lost some stem cell genes (e.g. *piwi*, *vasa*, and *tudor*)[29] but retained others (e.g. *argonaute*, *fgfr*)[9,10]. In larvae of the tapeworm *Echinococcus multilocularis*, many putative stem cell markers show limited overlapping gene expression patterns, pointing to a heterogenous cycling-cell population[10]. We depleted cycling cells in *H. diminuta* using irradiation and employed RNA-seq to uncover potential stem cell regulators in an unbiased fashion. Though irradiation may have secondary effects beyond stem cell depletion[23], this approach allowed us to generate an initial list of candidate tapeworm stem cell genes. Similar to other flatworms[23,30-32], we find that the cycling somatic cell population is heterogenous, though we also identified 23 genes, including *zmym3* and *su(Hw)*, that label all cycling cells in adult *H. diminuta*.

Importantly, we were able to use RNAi to functionally verify that cycling cell genes like *zmym3* and *su(Hw)* are critical for stem cell maintenance and that inhibition of these genes leads to impaired growth and regeneration. In other systems, *zmym3* has been shown to regulate cell cycle progression[33] and DNA repair[34], whereas *su(Hw)* binds to *gypsy* insulator sequences to regulate chromatin silencing[35]. Similar functions for these genes may be conserved in *H. diminuta* as cell cycle regulation, DNA repair, and chromatin silencing are likely important for the regulation of tapeworm stem cells. RNAi has been demonstrated previously in other tapeworm species[36-38], though not in *H. diminuta.* RNAi has not been widely adopted for studying tapeworm biology due to technical challenges like poor knockdown efficacy, inefficient penetrance, and the difficulty of *in vitro* culture. Taking advantage of the robust *in vitro* culture of *H. diminuta*, our RNAi scheme

285 can be expanded to ascertain functions for many parasitic flatworm genes that thus far have been
286 refractory to functional analyses.

287 Our screening strategy allowed us to verify 38 genes with enriched expression in some or
288 all cycling cells; however, none of these genes were expressed exclusively in the neck. Since we
289 had observed that regenerative ability was anteriorly biased across the neck, we attempted to
290 leverage this observation and query whether a subpopulation of pluripotent cycling cells may be
291 asymmetrically distributed across the neck and would be identifiable by RNA-seq. Through A-P
292 transcriptional profiling of the neck, we identified 461 anterior-enriched genes but the vast
293 majority of them were neither irradiation-sensitive nor detected in cycling cells by dFISH. Thus,
294 a subpopulation of neck-resident pluripotent stem cells, seems unlikely to explain the region-
295 specific regenerative ability of tapeworms. Nonetheless, our study does not exclude the existence
296 of a subpopulation of pluripotent stem cells that may be stably maintained in the adult. Future
297 studies using single-cell RNA sequencing are likely to provide a thorough characterization of adult
298 somatic stem cells in *H. diminuta*, as has been the case for planarians[31,32,39].

299 Is the neck competent to regenerate because of a unique stem cell population that has yet
300 to be identified, or because of signals extrinsic to stem cells that make the neck permissive for
301 regeneration? Tapeworms exposed to a lethal dose of irradiation prior to amputation are not
302 competent to regenerate and will eventually degenerate and die. However, transplantation of cells
303 from wild-type donors into the necks of irradiated tapeworms rescued lethality and regeneration.
304 This rescue ability is severely compromised if donor worms are first depleted of cycling cells using
305 drug treatment with HU, suggesting that some or all cycling cells have stem cell ability.
306 Interestingly, stem cell ability is not restricted to cells from regeneration-competent regions: cells
307 from posterior tissues that do not regenerate proglottids are still able to rescue regeneration when

transplanted into the neck. These data strongly suggest that the microenvironment within the neck confers regenerative ability to this region.

The interplay between intrinsic and extrinsic stem cell regulatory signals has been shown to play important roles in regeneration. Head regeneration was induced in three naturally regeneration-deficient planarian species by manipulating the gradient of Wnt signaling by RNAi[40-42]. These planarians maintain pluripotent stem cells but do not normally regenerate heads from posterior tissues due to inappropriately high levels of Wnt signaling, which inhibit anterior regeneration. As in planarians, gradients of Wnt signaling delineate A-P polarity in tapeworms[43]. Our transcriptional profiling of the neck A-P axis has already revealed hundreds of candidate genes with polarized expression profiles. Future experiments will help clarify how Wnt signaling and other A-P axis regulation in the neck impacts tapeworm regeneration.

Several plausible models can explain region-specific regeneration in *H. diminuta*. Head-dependent signals may create gradients across the neck that inhibit proglottidization and are necessary to maintain the neck as an unsegmented tissue. Proglottids can only form once the inhibitory signals are sufficiently diminished (Fig. 6d). In this model, the neck is competent to regenerate because of its juxtaposition to the head. After decapitation, the head-dependent signals eventually dissipate and segmentation signals dominate at the expense of the neck. The cellular source of the head-dependent signals and their molecular identity will be exciting avenues for future research.

In addition to its function in maintaining the neck, the head may also play a role in stem cell regulation (Fig. 6e). The head may regulate a niche (directly or indirectly) that is necessary for the maintenance of pluripotency in the neck. In this model, stem cells are collectively pluripotent only when they receive head-dependent niche signals, thus limiting regenerative

potential to the neck. Alternatively, stem cells may depend on a local niche that is independent of the head. In this model, stem cells have the capacity to form all cell lineages from any amputated fragment; however, the extrinsic signals that activate proglottid formation are restricted to the posterior neck region. Identifying the stem cell niche and its relationship to the head and neck microenvironment will provide crucial insights into our understanding of tapeworm regeneration.

Conclusion

Our study shows that *H. diminuta* is a powerful developmental model for understanding intrinsic and extrinsic regulation of stem cells and regeneration. The regionally limited regenerative biology of *H. diminuta* and the technical advances put forth in this work show that we can exploit this tapeworm to understand the complexities of stem cell regulation in parasites. We defined heterogenous stem cells that are collectively pluripotent but that require extrinsic head-dependent signals to enable persistent proglottid regeneration. Understanding how the stem cell niche we describe is regulated may have broad implications for elucidating stem cell biology in parasitic flatworms, as well as other regenerative animals.

Acknowledgements

We thank: members of the Newmark lab, especially Melanie Issigonis and Umair Khan, for discussions and comments on the manuscript; Alvaro Hernandez (Roy J. Carver Biotechnology Center, University of Illinois at Urbana-Champaign) for RNA-seq; and Bret Duffin (Morgridge Institute for Research) for invaluable assistance with irradiation. This work was supported by NIH R21AI119960. PAN is an investigator of the Howard Hughes Medical Institute.

Materials and Methods

Animal care and use

Infective *H. diminuta* cysts were obtained from Carolina Biological (132232). To obtain adult tapeworms, 100-400 cysts were fed to Sprague-Dawley rats by oral gavage in ~0.5 mL of 0.85% NaCl. Rats were euthanized in a CO_2 chamber 6 days post-gavage, tapeworms were flushed out of the small intestine, and washed in 1X Hanks Balanced Salt Solution (HBSS; Corning) (140 mg/L $CaCl_2$, 100 mg/L $MgCl_2.6H_2O$, 100 mg/L $MgSO_4.7H_2O$, 400 mg/L KCl, 60 mg/L KH_2PO_4, 350 mg/L $NaHCO_3$, 8 g/L NaCl, 48 mg/L Na_2HPO_4, 1 g/L D-glucose, no phenol red). Rodent care was in accordance with protocols approved by the Institutional Animal Care and Use Committee (IACUC) of the University of Wisconsin-Madison (M005573).

In vitro parasite culture

Biphasic parasite cultures were prepared based on the Schiller method[18]. Briefly, the solid phase was made in 50 mL Erlenmeyer flasks by mixing 30% heat-inactivated defibrinated sheep blood (Hemostat) with 70% agar base for 10 mL blood-agar mixture per flask. Fresh blood was heat-inactivated at 56°C for 30 min then kept at 4°C and used repeatedly for one week by first warming the blood to 37°C. The agar base was prepared from 8 g Difco nutrient agar and 1.75 g NaCl in 350 mL water, autoclaved, and stored at 4°C. Before use, the agar base was microwaved to liquify, and cooled to below 56°C before mixing with warmed blood. After the blood-agar mixture solidified, 10 mL of Working Hanks 4 (WH4; 1X HBSS/4 g/L total glucose/1X antibiotic-antimycotic (Sigma)) was added. Each flask was topped with a gas-permeable stopper (Jaece Identi-plug) and pre-incubated at 37°C in hypoxia (3% CO_2/5% O_2/92% N_2) overnight before use. Before tapeworms were transferred into the flasks, the liquid phase was adjusted to pH7.5 with 200 µL 7.5% $NaHCO_3$ (Corning). Tapeworms were first washed in WH4 for 10 mins at 37°C in

377 petri dishes pre-coated with 0.5% BSA to inhibit sticking. Transfers to pre-cultured flasks were
378 performed by gently lifting the worms with a stainless-steel hook (Moody Tools) and immersing
379 them in the liquid phase. Tapeworms were grown in hypoxia and transferred to fresh cultures every
380 3-4 days.

381 Fixation and DAPI Staining

382 Tapeworms were heat-killed by swirling in 75°C water for a few seconds until the worms
383 relaxed and elongated, then fixative (4% formaldehyde in Phosphate Buffered Saline with 0.3%
384 TritonX-100 (PBSTx)) was added immediately for 30 min-2hr at room temperature or overnight
385 at 4°C. For DAPI staining, samples were incubated in 1 µg/mL DAPI (Sigma) in PBSTx overnight
386 at 4°C and cleared in 80% glycerol/10 mM Tris pH7.5/1 mM EDTA overnight at room temperature
387 before mounting.

388 F-*ara*-EdU[31] uptake and staining

389 For F-*ara*-EdU pulse, tapeworms were incubated in 0.1 µM F-*ara*-EdU (Sigma) in 1%
390 DMSO at 37°C in WH4. Tapeworms were heat-killed (above) and fixed in 4% formaldehyde/10%
391 DMSO/1% NP40/PBSTx. Large tissues/worms were permeabilized by incubating in PBSTx at
392 room temp for several days. Additional permeabilization was achieved by treatment with 10
393 µg/mL Proteinase-K/0.1% SDS/PBSTx for 10-30 min at room temperature, fixed in 4%
394 formaldehyde/PBSTx for 10 min before samples were cut into small pieces or retained whole in
395 PBSTx. Samples were further permeabilized in PBSTx/10% DMSO/1% NP40 for 20min-1 hr
396 (depending on size) before performing the click-it reaction[44] with Oregon Green 488 Tyramide
397 (Invitrogen). Signal was detected using anti-Oregon Green 488-HRP antibody (1:1000;
398 Invitrogen) in K-block (5% Horse serum/0.45% fish gelatin/0.3% Triton-X/0.05% Tween-
399 20/PBS) [45] followed by Tyramide Signal Amplification (TSA) reaction [46]. Tiled confocal z-stacks

400 through the anterior of the worms were taken and cell numbers were counted using background
401 subtraction on Imaris software. F-*ara*-EdU^{+} cells were normalized to worm area from maximum
402 projections of the DAPI stain.

403 Irradiation

404 Most irradiation was performed using a CellRad irradiator (Faxitron Bioptics) at 200 Gy
405 (150 kV, 5 mA). Due to instrument failure, a cesium irradiator was used for one rescue experiment
406 with donors +/- HU (Fig. 6b) at 400 Gy (92±5 % cycling cell loss 3 days post-irradiation). In both
407 cases, lethal irradiation was determined as the dosage at which tapeworms degenerated and were
408 inviable after 30 days in culture. Irradiation was performed in WH4 in BSA-coated petri dishes.

409 Transcriptome assembly

410 RNA was collected from five regions: 1) head and neck, 2) immature proglottids, 3) mature
411 reproductive proglottids, 4) gravid proglottids, and 5) mixed larval stages isolated from beetles.
412 The first three regions covered the entirety of 3.5-week old adult tapeworms. Gravid proglottids
413 were taken from posteriors of 10-week old tapeworms. Paired-end libraries were constructed with
414 2 x 150 bp reads from a HiSeq2500 chip. 2 x ~30 million reads were obtained for each sample.
415 The transcriptome was assembled from three components: 1) map-based assembly, 2) *de novo*
416 assembly, and 3) Maker predictions from Wormbase Parasite. The map-based assembly was
417 performed using TopHat2 with the 2014 *H. diminuta* draft genome courtesy of Matt Berriman
418 (Wellcome Sanger Institute, UK). 15,859 transcripts were assembled using TopHat. *De novo*
419 assembly was performed using Velvet/Oases and resulted in 144,682 transcripts. There were
420 11,275 predicted Maker transcripts and 73.2% matched (>95% along the length) to the TopHat
421 transcripts. The remaining predicted transcripts that were not represented in the TopHat dataset
422 were added for a combined TopHat/predicted set of 17,651 transcripts. Most of the Oases

transcripts matched to the TopHat/predicted set but 35,300 or 24.4% of the Oases transcripts did not (>75% match cut-off). These transcripts could be transcripts missed in the genome, transcription noise, non-coding transcripts, or contamination. We found significant contamination from beetle tissue in the larval tapeworm sample (more below). Initial filtering for contamination excluded 1,388 transcripts (from beetle, rat, bacterial, and viral sources). At this point 51,563 transcripts were retained from the three methodologies described above and were processed for further filtering.

There was significant contamination from beetle tissues that had adhered to the tapeworm larvae, which produced transcripts with best hits to beetle proteins (*Ixodes scapularis, Harpegnathos saltator, Monodelphis domestica, Nasonia vitripennis, Pediculus humanus corporis, Solenopsis invicta, Tenebrio molitor,* or *Tribolium castaneum*). Most of the transcripts were from the Oases *de novo* assembly and did not match the *H. diminuta* genome. Furthermore, they were strongly over-represented in the larval sample only. To filter out beetle contamination, we removed 11,918 transcripts from the Oases assembly without matches to the *H. diminuta* genome that showed >90% expression (by RPKM) in the larval sample.

To the remaining 39,645 transcripts, we applied additional filters: 1) Remove transcripts if average RPKM<1 unless the transcript is long (>1000 bp), has a long ORF (>500 bp) or is annotated. 11,615 transcripts were removed as they met none of these criteria. 2) A stringent expression cut-off was applied to the remaining Oases transcripts; transcripts were discarded if average RPKM<5 and maximum RPKM<10 unless the transcripts were long (>1000 bp), had long ORFs (>500 bp) or were annotated. 8,027 transcripts were removed. 3) 51 transcripts were removed because they are mitochondrial or rRNAs. 4) An ORF size filter was applied to remove all transcripts with ORF <300 bp unless they are annotated. 5,331 transcripts were removed. 5)

For the Maker predicted transcripts, expression and size filters were applied to remove transcripts with expression <1 RPKM and size <500 bp. 275 transcripts were removed.

Our final transcriptome is comprised of 14,346 transcripts (84.9% TopHat, 8.4% Maker predictions, 6.1% Oases with match to genome, and 0.6% Oases without match to genome). The total transcriptome size is 34 Mb with average transcript length of 2,354 bp.

RNA-seq for differential gene expression analyses

Tissue was collected and immediately frozen on dry ice in 100 µL Trizol (Life Technologies) before RNA extraction. Tissue homogenization was performed as the mixture was in a semi-frozen state using RNase-free pestles and a pestle motor. RNA was purified using the Direct-zol RNA MiniPrep kit (Zymo). RNA quality was assessed using Bioanalyzer, libraries were prepared with TruSeq Stranded mRNAseq Sample Prep kit (Illumina), and sequenced on two lanes on a HiSeq2500 chip. We performed paired-end sequencing and obtained ~20 million reads per sample. Samples were obtained in triplicate. To identify irradiation-sensitive genes, 2 mm anterior tapeworm fragments were cut from 10 worms after 3 days *in vitro*. To identify differentially expressed transcripts across the neck A-P axis, 1 mm fragments were cut from 20 freshly obtained 6-day old tapeworms. Differential gene expression analysis was performed using CLC Genomics Workbench (Qiagen) by mapping to our assembled transcriptome (above).

Cloning

Target genes were amplified using PCR with Platinum Taq (Life Technologies) from cDNA generated from RNAs extracted from tapeworm anteriors to enrich for neck transcripts. PCR products were inserted via TA-mediated cloning into the previously described vector pJC53.2[47] pre-digested with *Eam11051*. Anti-sense riboprobes could be generated by *in vitro*

468 transcription with SP6 or T3 RNA polymerases. For RNAi, dsRNA was generated using T7 RNA
469 polymerase. For sequences and primers, refer to Supplemental Table 4.

470 *In situ* hybridization

471 WISH and FISH protocols were modified from previously published methods for
472 planarians[46] and the mouse bile-duct tapeworm *Hymenolepis microstoma* [48]. Tapeworms were heat
473 killed and fixed in 4% formaldehyde/10% DMSO/1% NP40/PBSTx for 30 min at room
474 temperature before washing and dehydration into methanol. Dehydrated samples were frozen at -
475 30°C for at least 2 days. After rehydration, samples were permeabilized in 10 µg/mL Proteinase-
476 K/0.1% SDS/PBSTx for 30 min, washed into 0.1 M Triethanolamine pH7-8 (TEA), 2.5 µL/mL
477 acetic anhydride was added for 5 min with vigorous swirling, acetic anhydride step was repeated,
478 washed in PBSTx, and post-fixed in 4% formaldehyde/PBSTx for 10 min. Probe synthesis,
479 hybridization, and staining were performed as previously described[46] using probe concentrations
480 at ~50 ng/mL for 16-48 hrs at 56°C. All probes were synthesized with either DIG or DNP haptens
481 and detected using the following antibodies, all at 1:2000: anti-DIG-AP (Sigma), anti-DIG-POD
482 (Roche), anti-DNP-HRP (Vector Labs). Colorimetric development was done using NBT
483 (Roche)/BCIP (Sigma) or with Fast-Blue (Sigma)[49]. Fluorescent signal was visualized after TSA
484 reaction[46]. DAPI staining and mounting were performed as described above.

485 Imaging

486 Confocal imaging was performed on a Zeiss LSM 880 with the following objectives:
487 20X/0.8 NA Plan-APOCHROMAT, 40X/1.3 NA Plan-APOCHROMAT, and 63X/1.4 NA Plan-
488 APOCHROMAT. WISH samples and whole-mount DAPI-stained worms were imaged using
489 Zeiss AxioZoom V16 macroscope. Image processing was performed using ImageJ for general
490 brightness/contrast adjustments, maximum-intensity projections, and tile stitching[50].

491 RNAi

492 dsRNA was synthesized as previously described[51] and resuspended at concentrations ~ 1.5-
493 2 µg/µL. For control injections, 1.5 kb dsRNA derived from *ccdB* and *camR*-containing insert of
494 the pJC53.2 vector was used[47]. 6-day old tapeworms were obtained and microinjected with dsRNA
495 using femtotips II via the Femtojet injection system (Eppendorf) to obtain spreading across the
496 first ~ 3-4 mm anterior of the tapeworm. The spread of injected fluids could be detected by a
497 temporary increase in opacity. 500 hPa injection pressure for 0.3-1 s was used per injection site.
498 Whole tapeworms were cultured *in vitro* for 3 days, 2 mm anterior fragments were amputated,
499 worms were re-injected with dsRNA on day 6, and cultured *in vitro* for an additional 9 days before
500 termination.

501 qPCR for target gene knockdown efficacy

502 Whole worms (6-days old) were injected with dsRNA throughout and frozen in Trizol on
503 dry ice after 6 days *in vitro* for RNA extraction according to manufacturer's protocol and DNAse
504 (Promega) treatment for 30 min at 37°C. cDNA synthesis was performed using SuperScriptIII
505 First-Strand Synthesis System (Invitrogen) with Oligo$(dT)_{20}$ primers followed by iScript cDNA
506 Synthesis Kit (Bio-Rad). qPCR was performed using GoTaq Mastermix (Promega) on a
507 StepOnePlus real-time PCR machine (Applied Biosystems). *60S ribosomal protein L13*
508 (*60Srpl13)* was used as an internal normalization control. For primers refer to Supplemental Table
509 4.

510 Hydroxyurea (HU) treatment

511 Tapeworms were treated with HU (Sigma) or HBSS (for controls) every day for a total of
512 6 days. HU stock solution was made fresh every day at 2 M in HBSS. 250 µL was added to each
513 flask of tapeworms for final concentration of 50 mM. HU is unstable at 37°C so worms were

514 transferred into fresh HU-containing media every two days, and fresh HU was added every other
515 day.

516 Cell transplantations

517 For dissociated cell preparations, tapeworms were placed in a drop of calcium-magnesium
518 free HBSS (CMF HBSS, Gibco), minced into small pieces with a tungsten needle, incubated in
519 3X Trypsin-EDTA (Sigma) in CMF HBSS for 30 min at 37°C and dissociated using a dounce
520 homogenizer (Kontes). Cells were pelleted by centrifugation at 250 g for 5 min. The cell pellet
521 was washed in CMF HBSS and passed through cell strainers at 100 μm, 40 μm, 20 μm, and 10
522 μm (Falcon and Sysmex) with one spin and wash in between. Cells were pelleted and resuspended
523 in 200-400 μL WH4 with 0.05% BSA. Cell injections were performed using the Cell Tram Oil 4
524 injection system (Eppendorf) into the necks of irradiated worms. For +/- HU donors, cell
525 concentrations were measured using a hemocytometer and normalized (to ~10^8 cells/mL) to ensure
526 equal numbers of cells were injected. After 3 days *in vitro,* 5 mm anterior fragments were
527 amputated and grown for an additional 27 days.

528 Statistical Analysis.

529 Statistical analyses were performed using Prism7 software (GraphPad Prism). All
530 experiments were repeated at least twice. All measurements were taken from distinct samples.
531 Error bars, statistical tests, number of replicates (N) and sample sizes (n) are indicated in
532 corresponding figure legends. Either Dunnett's or Tukey's multiple comparison tests were used
533 for one-way ANOVAs based on Prism recommendation. SD=standard deviation. P-values: ns=
534 not significant, *= $p \leq 0.5$, ****= $p \leq 0.0001$.
535

References

1. Del Brutto, O. H. Human cysticercosis (*Taenia solium*). *Trop Parasitol* **3,** 100–103 (2013).
2. Craig, P. & Ito, A. Intestinal cestodes. *Curr. Opin. Infect. Dis.* **20,** 524–532 (2007).
3. Roberts, L. S. Development of *Hymenolepis diminuta* in its definitive host in *Biology of the Tapeworm Hymenolepis diminuta* 357–423 (Academic Press Inc., NY, 1980).
4. Arai, H. P. (Ed.) *Biology of the Tapeworm Hymenolepis diminuta*. (Academic Press, Inc., 1980).
5. Read, C. P. Longevity of the tapeworm, *Hymenolepis diminuta*. *J. Parasitol.* **53,** 1055–1056 (1967).
6. Newmark, P. A. & Sánchez Alvarado, A. Not Your Father's Planarian: A Classic Model Enters The Era Of Functional Genomics. *Nat. Rev. Genet.* **3,** 210–219 (2002).
7. Reddien, P. W. The Cellular and Molecular Basis for Planarian Regeneration. *Cell* **175,** 327–345 (2018).
8. Baguñà, J. The planarian neoblast: the rambling history of its origin and some current black boxes. *Int. J. Dev. Biol.* **56,** 19–37 (2012).
9. Collins, J., III *et al.* Adult somatic stem cells in the human parasite *Schistosoma mansoni*. *Nature* **494,** 476–479 (2013).
10. Koziol, U., Rauschendorfer, T., Zanon Rodríguez, L., Krohne, G. & Brehm, K. The unique stem cell system of the immortal larva of the human parasite *Echinococcus multilocularis*. *EvoDevo* **5,** 10 (2014).
11. Koziol, U. *et al.* A Novel Terminal-Repeat Retrotransposon in Miniature (TRIM) Is Massively Expressed in *Echinococcus multilocularis* Stem Cells. *Genome Biol Evol* **7,** 2136–2153 (2015).
12. Wang, B., Collins, J., III & Newmark, P. A. Functional genomic characterization of neoblast-like stem cells in larval *Schistosoma mansoni*. *Elife* **2,** e00768 (2013).
13. Koziol, U., Domínguez, M. F., Marín, M., Kun, A. & Castillo, E. Stem cell proliferation during in vitro development of the model cestode *Mesocestoides corti* from larva to adult worm. *Front. Zool.* **7,** 22 (2010).
14. Collins, J., III. Platyhelminthes. *Current Biology* **27,** R252–R256 (2017).
15. Collins, J., III, Wendt, G. R., Iyer, H. & Newmark, P. A. Stem cell progeny contribute to the schistosome host-parasite interface. *Elife* **5,** 243 (2016).
16. Brehm, K. & Koziol, U. On the importance of targeting parasite stem cells in anti-echinococcosis drug development. *Parasite* **21,** 72 (2014).
17. Rozario, T. & Newmark, P. A. A confocal microscopy-based atlas of tissue architecture in the tapeworm *Hymenolepis diminuta*. *Exp. Parasitol.* **158,** 31–41 (2015).
18. Schiller, E. L. A simplified method for the in vitro cultivation of the rat tapeworm, *Hymenolepis diminuta*. *J. Parasitol.* **51,** 516–518 (1965).
19. Goodchild, C. G. Transfaunation and Repair of Damage in the Rat Tapeworm, *Hymenolepis diminuta*. *J. Parasitol.* **44,** 345–351 (1958).
20. Bolla, R. I. & Roberts, L. S. Developmental physiology of cestodes. IX. Cytological characteristics of the germinative region of *Hymenolepis diminuta*. *J. Parasitol.* **57,** 267–277 (1971).

21. Sulgostowska, T. The development of organ systems in cestodes. I. A study of histology of *Hymenolepis diminuta* (Rudolphi, 1819)(Hymenolepididae). *Acta Parasitologica Polonica* **20,** 449–462 (1972).
22. Neef, A. B. & Luedtke, N. W. Dynamic metabolic labeling of DNA in vivo with arabinosyl nucleosides. *Proceedings of the National Academy of Sciences* **108,** 20404–20409 (2011).
23. Solana, J. *et al.* Defining the molecular profile of planarian pluripotent stem cells using a combinatorial RNAseq, RNA interference and irradiation approach. *Genome Biol.* **13,** R19 (2012).
24. Eisenhoffer, G. T., Kang, H. & Sánchez Alvarado, A. Molecular Analysis of Stem Cells and Their Descendants during Cell Turnover and Regeneration in the Planarian *Schmidtea mediterranea*. *Cell Stem Cell* **3,** 327–339 (2008).
25. Koziol, U. & Castillo, E. Cell proliferation and differentiation in cestodes. *Research in Helminths* 121–138 (2011).
26. Collins, J. N. R. & Collins, J., III. Tissue Degeneration following Loss of *Schistosoma mansoni* cbp1 Is Associated with Increased Stem Cell Proliferation and Parasite Death In Vivo. *PLoS Pathog* **12,** e1005963 (2016).
27. Cheever, A. W., Macedonia, J. G., Mosimann, J. E. & Cheever, E. A. Kinetics of Egg Production and Egg Excretion by *Schistosoma mansoni* and *S. japonicum* in Mice Infected with a Single Pair of Worms. *The American Journal of Tropical Medicine and Hygiene* **50,** 281–295 (1994).
28. Lumsden, R. D. & Specian, R. The morphology, histology, and fine structure of the adult stage of the cyclophyllidean tapeworm *Hymenolepis diminuta* in *Biology of the Tapeworm Hymenolepis diminuta.* 157–280 (Academic Press Inc., NY, 1980).
29. Tsai, I. J. *et al.* The genomes of four tapeworm species reveal adaptations to parasitism. *Nature* **496,** 57–63 (2013).
30. van Wolfswinkel, J. C., Wagner, D. E. & Reddien, P. W. Single-Cell Analysis Reveals Functionally Distinct Classes within the Planarian Stem Cell Compartment. *Cell Stem Cell* **15,** 326–339 (2014).
31. Fincher, C. T., Wurtzel, O., de Hoog, T., Kravarik, K. M. & Reddien, P. W. Cell type transcriptome atlas for the planarian Schmidtea mediterranea. *Science* **360,** eaaq1736 (2018).
32. Zeng, A. *et al.* Prospectively Isolated Tetraspanin+ Neoblasts Are Adult Pluripotent Stem Cells Underlying Planaria Regeneration. *Cell* **173,** 1593–1608.e20 (2018).
33. Hu, X. *et al.* Gene knockout of *Zmym3* in mice arrests spermatogenesis at meiotic metaphase with defects in spindle assembly checkpoint. *Cell Death Dis* **8,** e2910 (2017).
34. Leung, J. W. C. *et al.* ZMYM3 regulates BRCA1 localization at damaged chromatin to promote DNA repair. *Genes Dev.* **31,** 260–274 (2017).
35. Gdula, D. A., Gerasimova, T. I. & Corces, V. G. Genetic and molecular analysis of the gypsy chromatin insulator of Drosophila. *Proc. Natl. Acad. Sci. U.S.A.* **93,** 9378–9383 (1996).
36. Pierson, L. *et al.* RNA interference in a cestode reveals specific silencing of selected highly expressed gene transcripts. *Int. J. Parasitol.* **40,** 605–615 (2010).
37. Mizukami, C. *et al.* Gene silencing in *Echinococcus multilocularis* protoscoleces using RNA interference. *Parasitol. Int.* **59,** 647–652 (2010).

38. Spiliotis, M. *et al. Echinococcus multilocularis* primary cells: improved isolation, small-scale cultivation and RNA interference. *Mol. Biochem. Parasitol.* **174,** 83–87 (2010).
39. Plass, M. *et al.* Cell type atlas and lineage tree of a whole complex animal by single-cell transcriptomics. *Science* **360,** eaaq1723 (2018).
40. Sikes, J. M. & Newmark, P. A. Restoration of anterior regeneration in a planarian with limited regenerative ability. *Nature* **500,** 77–80 (2013).
41. Liu, S. Y. *et al.* Reactivating head regrowth in a regeneration-deficient planarian species. *Nature* **500,** 81–84 (2013).
42. Umesono, Y. *et al.* The molecular logic for planarian regeneration along the anterior-posterior axis. *Nature* **500,** 73–76 (2013).
43. Koziol, U., Jarero, F., Olson, P. D. & Brehm, K. Comparative analysis of Wnt expression identifies a highly conserved developmental transition in flatworms. *BMC Biol.* **14,** 1 (2016).
44. Salic, A. & Mitchison, T. J. A chemical method for fast and sensitive detection of DNA synthesis in vivo. *Proceedings of the National Academy of Sciences* **105,** 2415–2420 (2008).
45. Collins, J., III, King, R. S., Cogswell, A., Williams, D. L. & Newmark, P. A. An atlas for *Schistosoma mansoni* organs and life-cycle stages using cell type-specific markers and confocal microscopy. *PLoS Negl Trop Dis* **5,** e1009 (2011).
46. King, R. S. & Newmark, P. A. In situ hybridization protocol for enhanced detection of gene expression in the planarian *Schmidtea mediterranea*. *BMC Dev. Biol.* **13,** 8 (2013).
47. Collins, J., III *et al.* Genome-wide analyses reveal a role for peptide hormones in planarian germline development. *PLoS Biol.* **8,** e1000509 (2010).
48. Olson, P. D. *et al.* Genome-wide transcriptome profiling and spatial expression analyses identify signals and switches of development in tapeworms. *EvoDevo* **9,** R991 (2018).
49. Currie, K. W. *et al.* HOX gene complement and expression in the planarian *Schmidtea mediterranea*. *EvoDevo* **7,** 7 (2016).
50. Preibisch, S., Saalfeld, S. & Tomancak, P. Globally optimal stitching of tiled 3D microscopic image acquisitions. *Bioinformatics* **25,** 1463–1465 (2009).
51. Rouhana, L. *et al.* RNA interference by feeding in vitro-synthesized double-stranded RNA to planarians: methodology and dynamics. *Dev. Dyn.* **242,** 718–730 (2013).

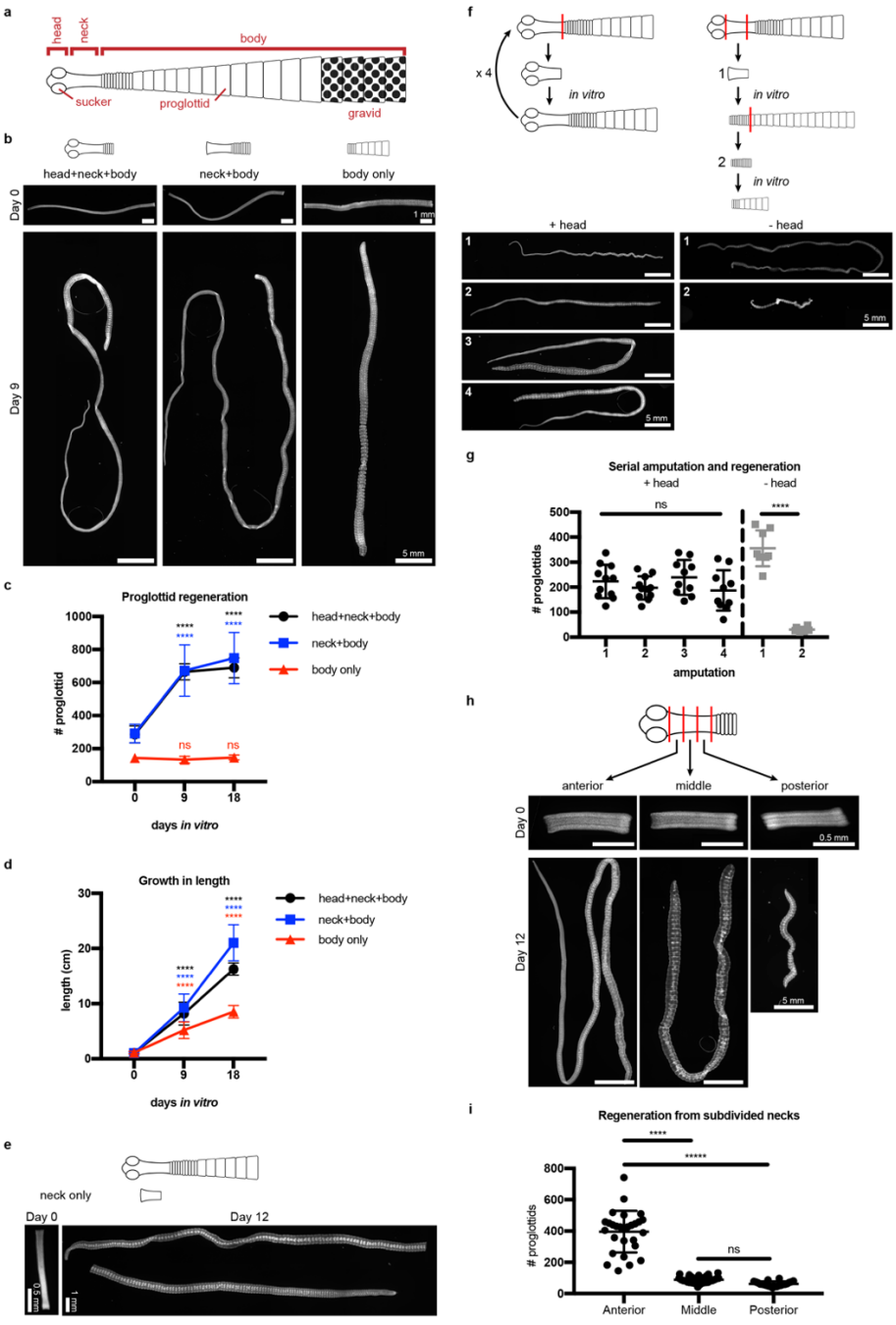

Figure 1. Regeneration competence of *H. diminuta*. **a**, Schematic of *H. diminuta* adults. **b**, DAPI-stained 1 cm fragments grown *in vitro*. **c-d**, Quantification of proglottid number and growth in length from (**b**). Error bars=SD, N=2-5, n=7-21; one-way ANOVA with Dunnett's multiple comparison test, compared to Day 0. **e**, Representative DAPI-stained "neck only" fragment regeneration. **f-g**, 2 mm anterior fragments, with or without the head, grown *in vitro* for 12-15 days and then re-amputated serially. Error bars=SD, +head: one-way ANOVA with Tukey's multiple comparison test, -head: Student's t-test. **h-i**, DAPI-stained 1 mm fragments from the anterior, middle, and posterior of the neck grown *in vitro*. Error bars=SD, N=3, n=22-29, one-way ANOVA with Tukey's multiple comparison test.

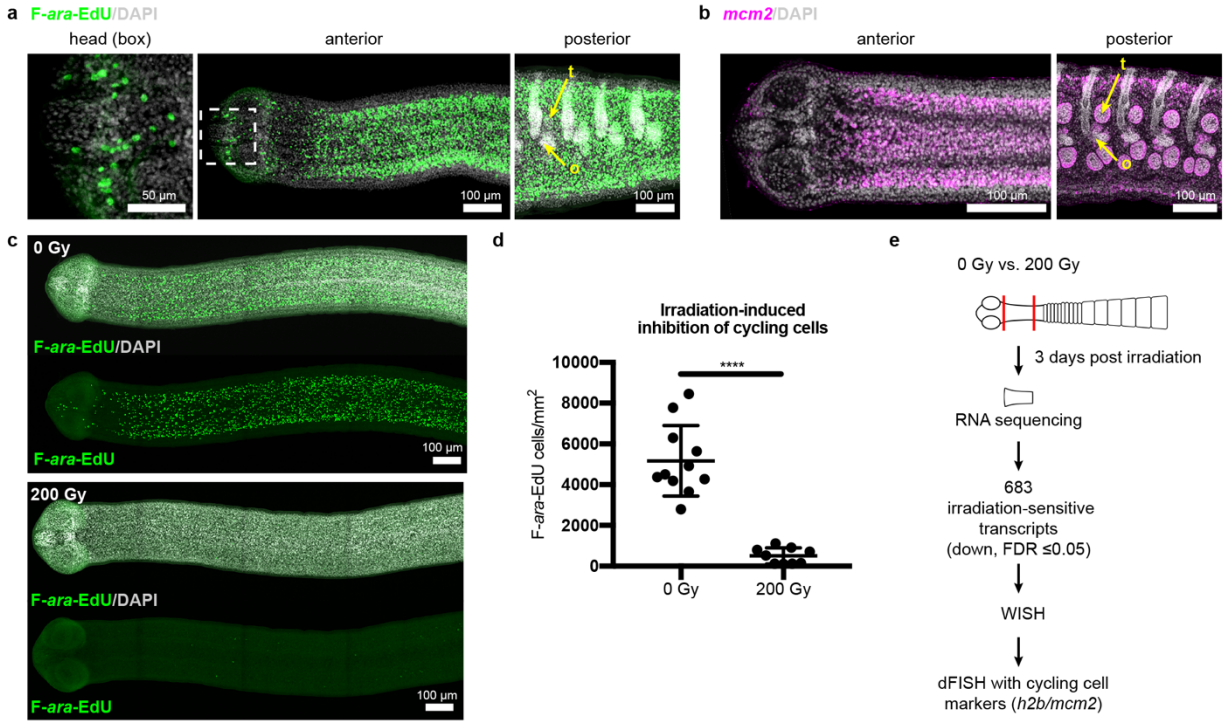

Figure 2. Cycling somatic cells are distributed throughout the tapeworm body and are irradiation sensitive. a-b, Maximum-intensity projections of confocal sections showing distribution of cycling cells by 2 hr uptake of F-*ara*-EdU (**a**) or FISH for *mcm2* (**b**). Fewer cycling cells were found in the head (box), while abundant cycling cells were observed in both somatic and gonadal tissues throughout the body. t=testis, o=ovary. **c**, Maximum-intensity projections of tile-stitched confocal sections after 1 hr uptake of F-*ara*-EdU (green) 3 days post-irradiation. **d**, Quantification of F-*ara*-EdU^{+} cell inhibition from (**c**). Error bars=SD, N=2, n=11 and 9, Student's t-test. **e**, RNA-seq strategy to identify genes expressed in cycling cells.

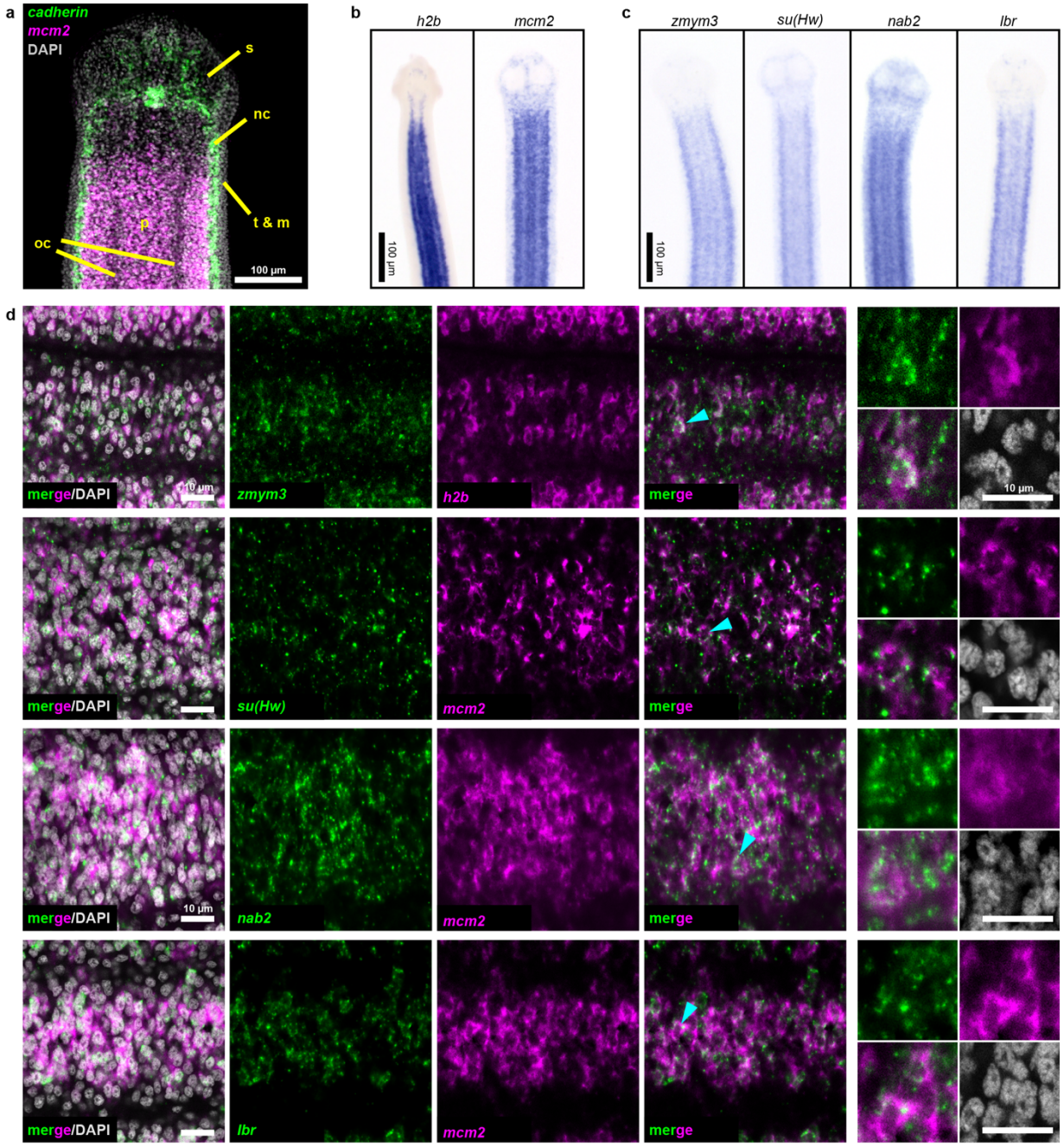

Figure 3. Expression screening for cycling cell markers. a, Confocal section of a tapeworm anterior. Cycling cells (*mcm2*: magenta) in the neck parenchyma between the nerve cords (*cadherin*: green). s: sucker, nc: nerve cord, oc: osmoregulatory canal, t: tegument, m: muscle, and p: parenchyma. **b**, WISH of known cycling-cell markers *h2b* and *mcm2*. **c**, WISH for irradiation-sensitive genes expressed in the neck parenchyma. **d**, Confocal sections of dFISH for irradiation-sensitive genes (green) with *h2b* or *mcm2* (magenta) from neck parenchyma. Cyan arrowheads indicate cells magnified at the far right.

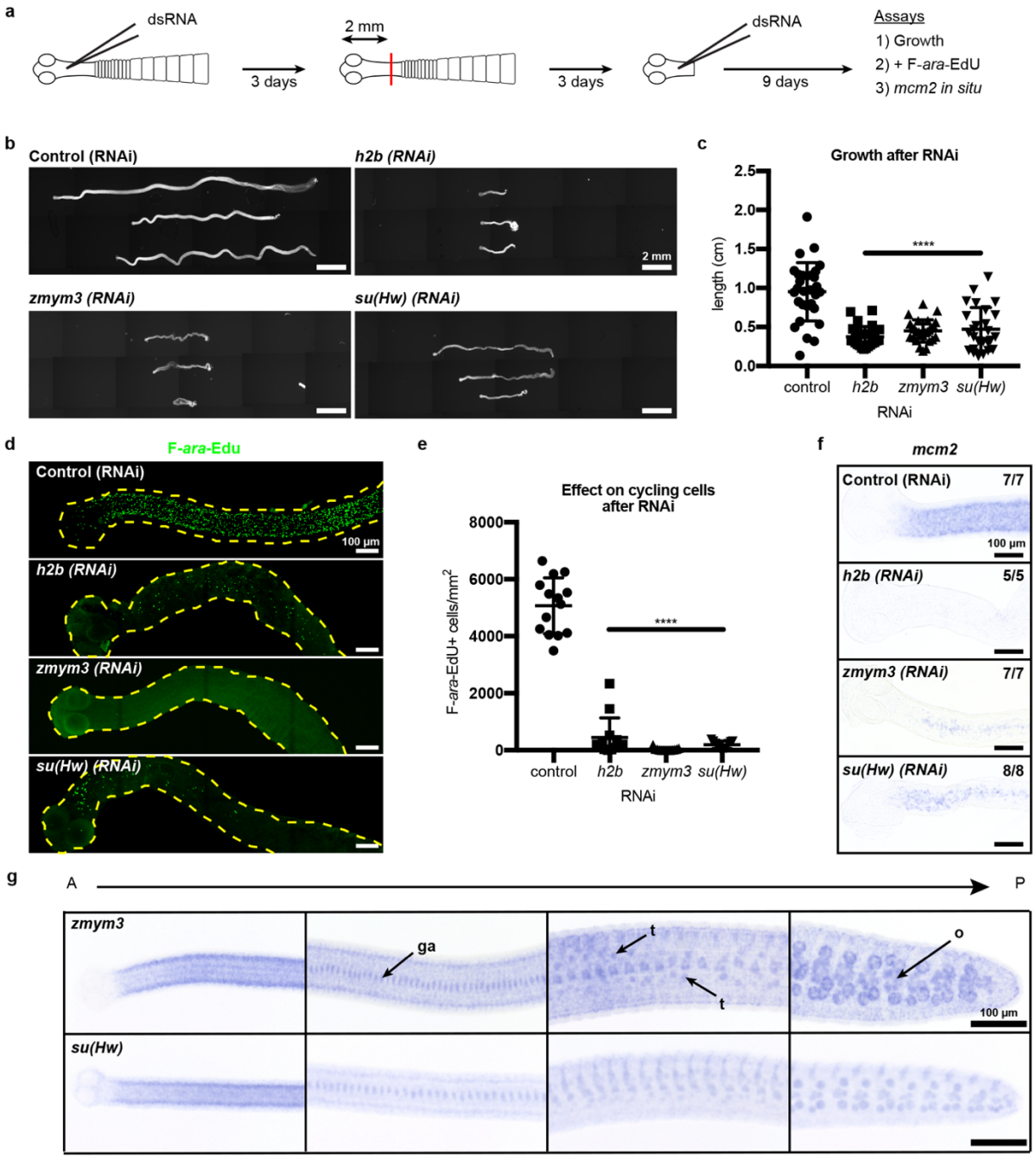

Figure 4. RNAi to identify genes required for growth and regeneration in *H. diminuta*. **a**, Schematic of RNAi paradigm. **b**, DAPI-stained worms after RNAi knockdown of *h2b, zmym3*, and *su(Hw)*. **c**, Quantification of worm lengths after RNAi. Error bars=SD, N=3-4, n=26-37, one-way ANOVA with Dunnett's multiple comparison test compared to control. **d-e**, Maximum-intensity projections (**d**) and quantification (**e**) of cycling-cell inhibition after 1 hr F-*ara*-EdU uptake following RNAi. Worms with degenerated necks were excluded from analysis. Error bars=SD, N=3, n=11-14, one-way ANOVA with Dunnett's multiple comparison test compared to control. **f**, *mcm2* WISH on worm anteriors after RNAi. **g**, WISH of *zmym3* and *su(Hw)* sampled from anterior to posterior of adult 6-day old worms. ga: genital anlagen; t: testis; o: ovary.

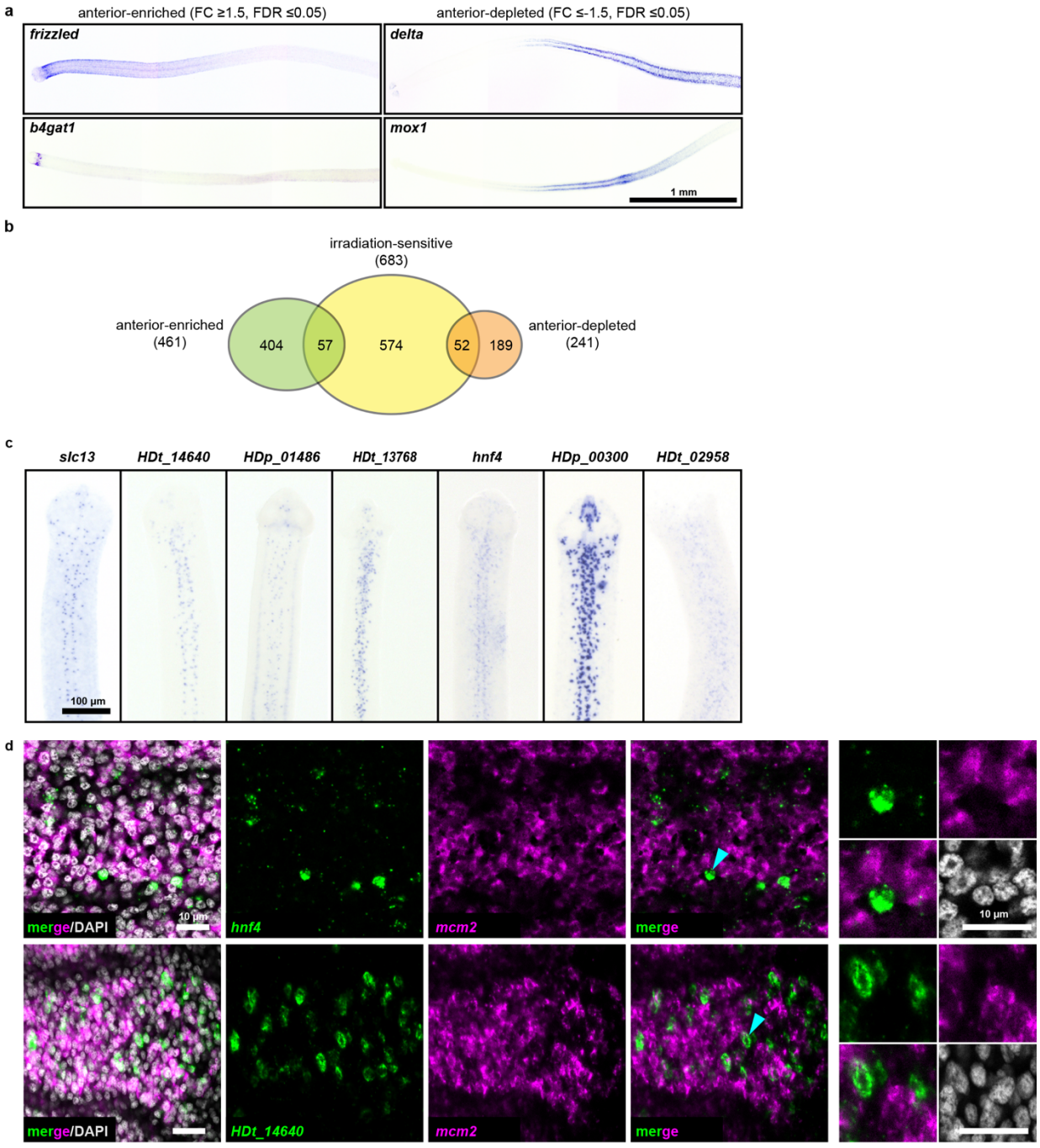

Figure 5. RNA-seq identifies anterior-enriched genes that are expressed predominantly in non-cycling cells. a, WISH of tapeworm anteriors for genes that were anterior-enriched (FC ≥1.5, FDR ≤0.05) or -depleted (FC ≤-1.5, FDR ≤0.05) by RNA-seq. Panels oriented anterior facing left. **b,** Differential gene expression analyses of 1 mm anterior, middle, and posterior neck fragments overlaid with irradiation-sensitive transcripts. **c**, WISH of genes that were anterior-enriched and irradiation-sensitive by RNA-seq that showed expression in a subset of cells in the neck parenchyma. **d**, Confocal sections from dFISH of anterior-enriched genes (green) and *mcm2* (magenta). Cyan arrowheads indicate cells that are magnified at the far right.

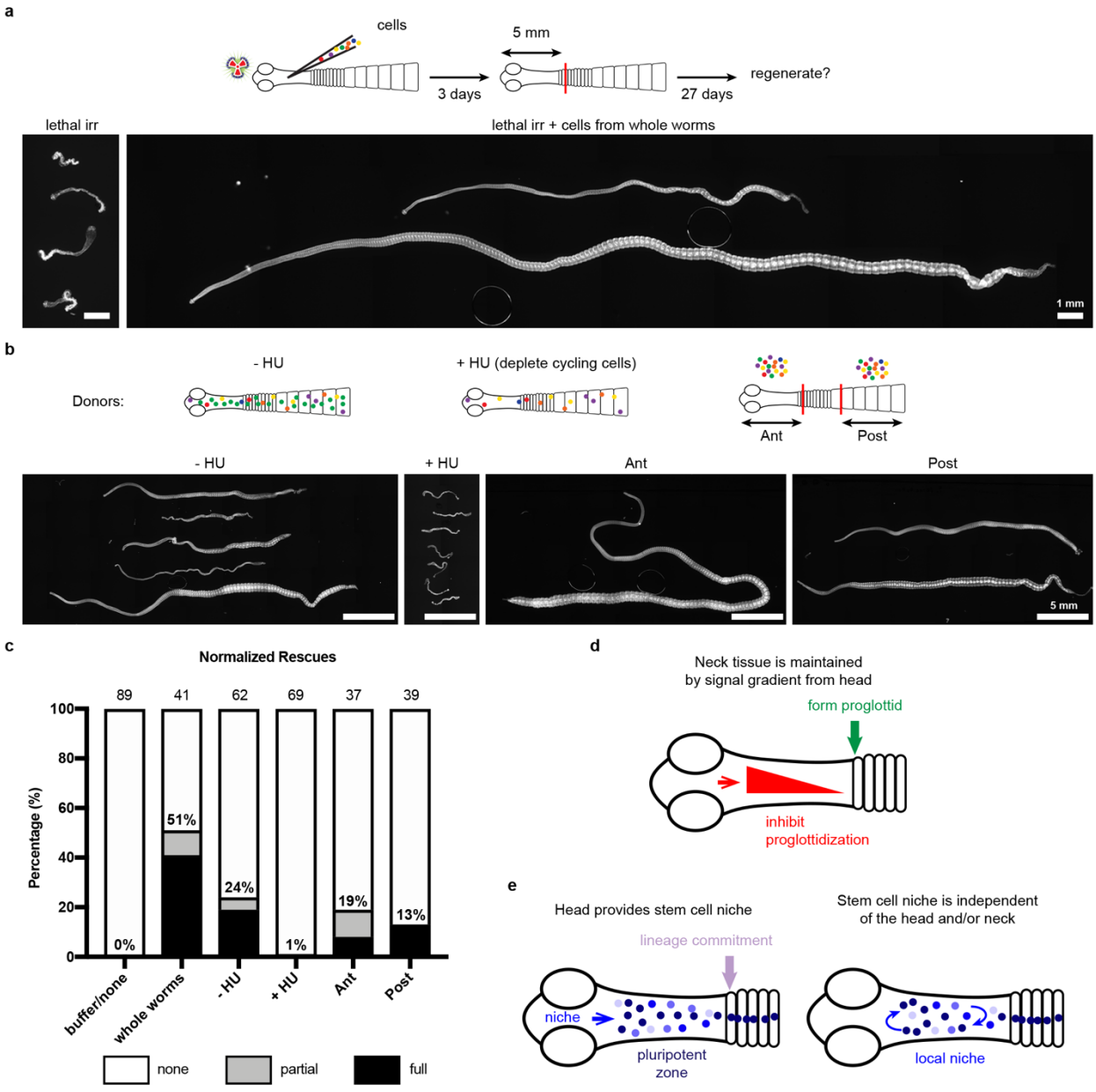

Figure 6. Stem cell activity depends on cycling cells but is not confined to cells from the neck. **a-b**, DAPI-stained worms after rescue with cell transplantations from whole-worm donors (**a**) or sourced from depicted donors (**b**). **c**, Quantification of rescue phenotypes from pooled experiments. Number of animals listed above bars. **d**, Model for head-dependent neck maintenance and proglottid formation. **e**, Models of head-dependent or -independent stem cell niches.

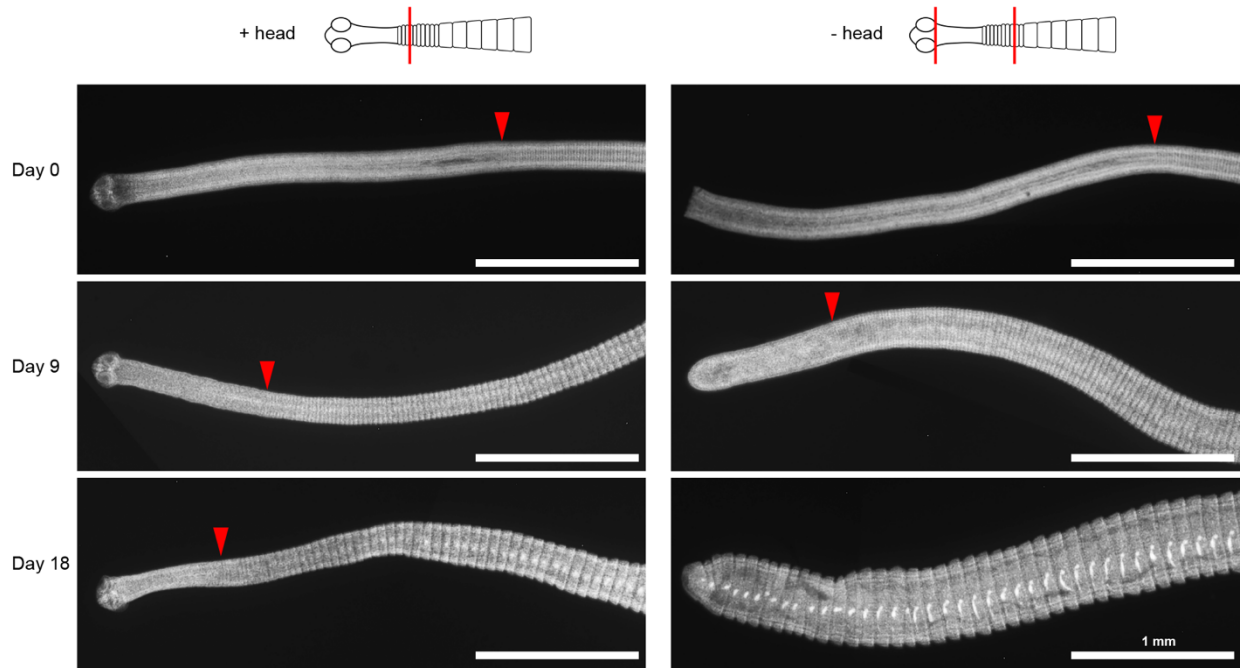

708

709 **Figure 1–figure supplement 1. Unsegmented neck is depleted after decapitation.** DAPI-
710 stained worms with or without decapitation were cultured *in vitro* for the indicated number of days.
711 Red arrowheads mark the position of the first visible proglottid. After 18 days *in vitro,* the neck
712 tissue is no longer identifiable in -head worms.

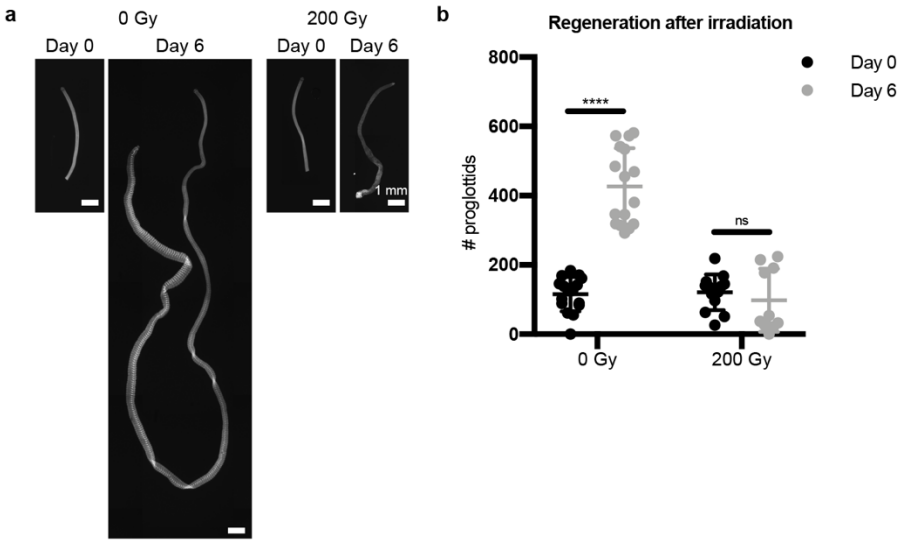

Figure 2–figure supplement 1. Irradiation inhibits tapeworm regeneration. a, DAPI staining of 5 mm anterior fragments from control and irradiated worms before and after 6 days *in vitro* culture. **b**, Quantification of **(a)**. Error bars=SD, N=2, n= 10-16, one-way ANOVA with Tukey's multiple comparison test.

719

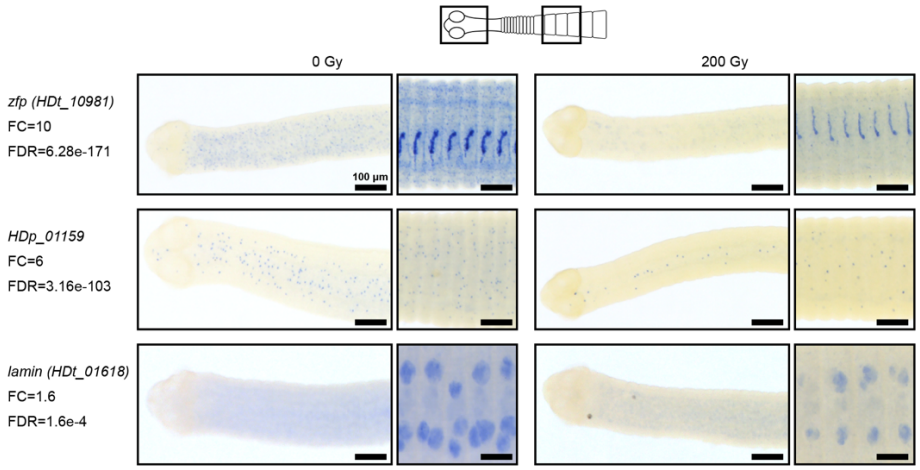

720

721 **Figure 2–figure supplement 2. Validation of RNA-seq by WISH after irradiation.** WISH (with
722 Fast-Blue Development) from two regions of the tapeworm: anterior (left) and body (right), 3 days
723 post-irradiation.

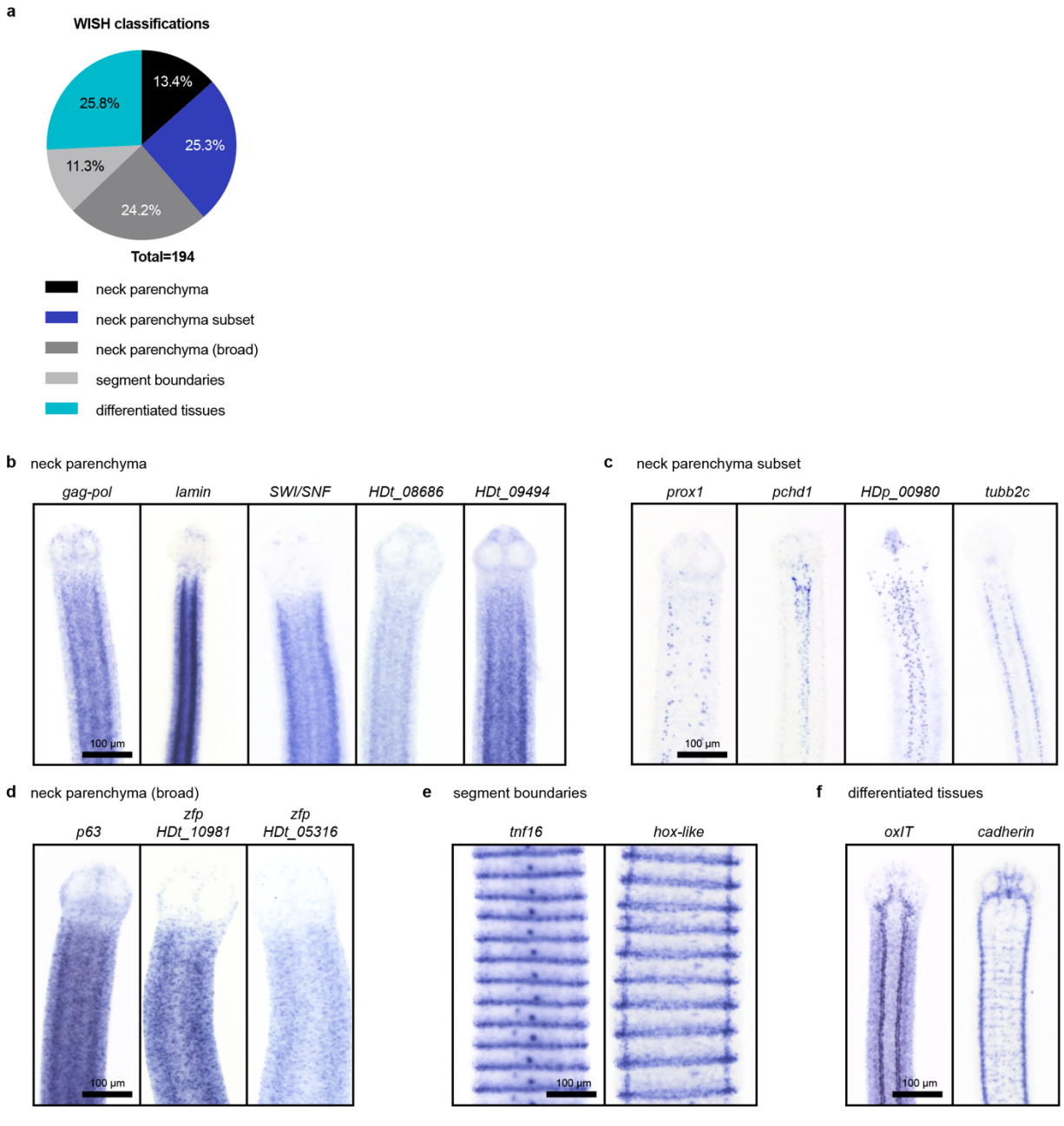

Figure 3–figure supplement 1. WISH patterns of irradiation-sensitive genes identified using RNA-seq. a, Classification of WISH expression patterns of irradiation-sensitive genes. **b-f**, Examples of genes expressed in the neck parenchyma (**b**), in subsets of cells within the neck (**c**), in neck parenchyma and broadly toward the animal edge where differentiated muscle and tegument are located (**d**), at segment boundaries (**e**), and in differentiated tissues (**f**) like the osmoregulatory canals (left) and nervous system (right).

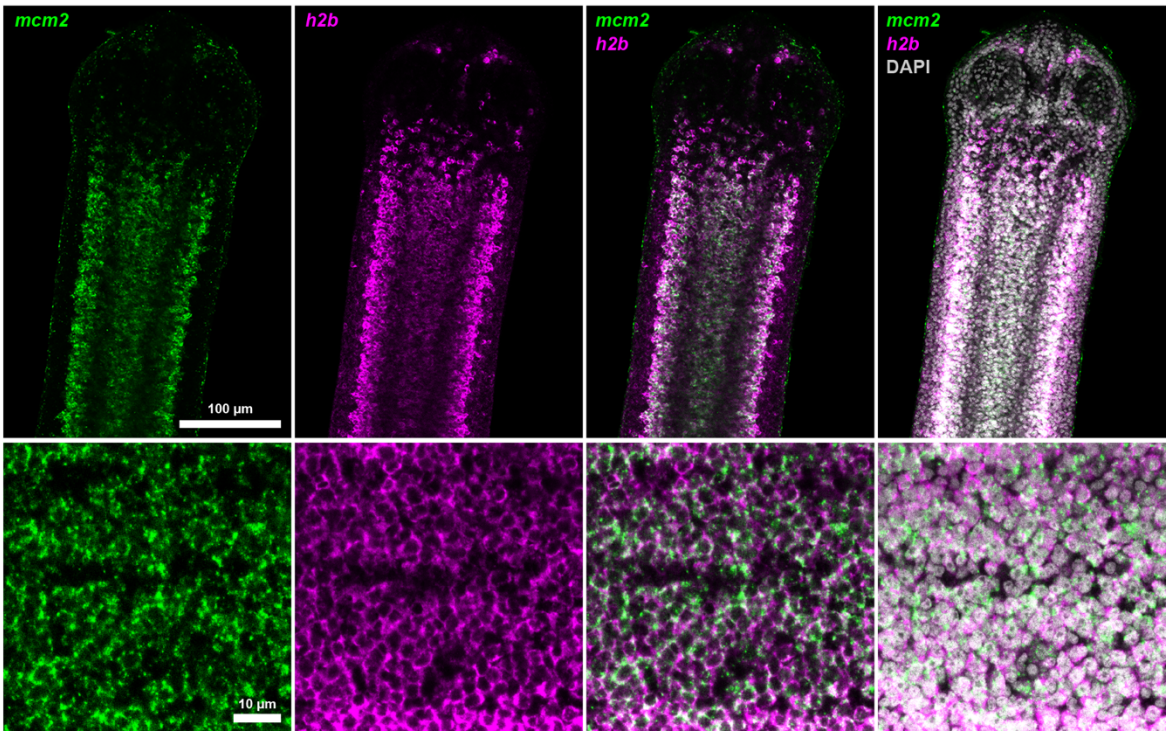

Figure 3–figure supplement 2. Colocalization of *mcm2* and *h2b*. Confocal section of dFISH to detect *mcm2* (green) and *h2b* (magenta) in the neck parenchyma at low(top) and high (bottom) magnification.

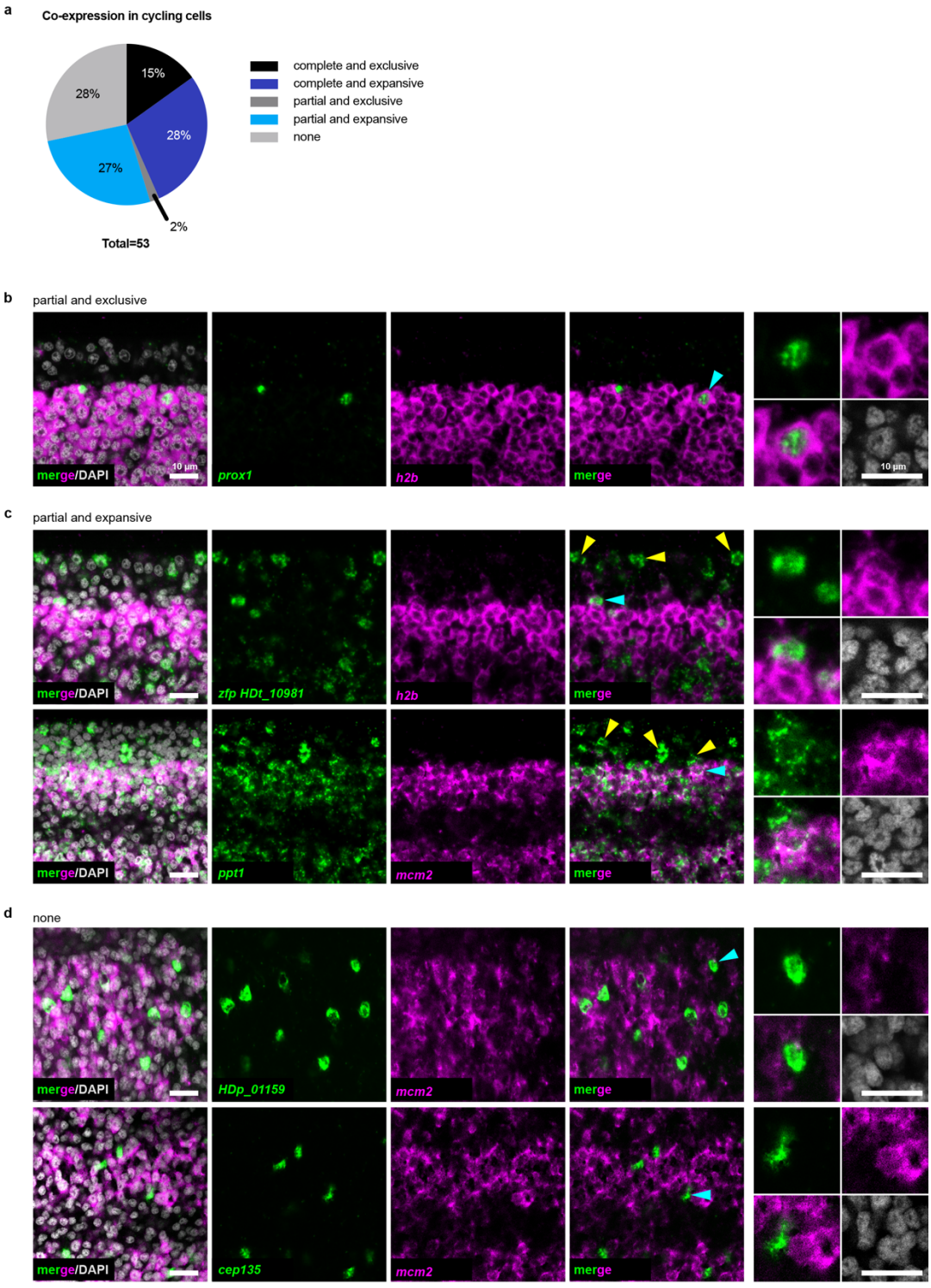

Figure 3–figure supplement 3. The cycling somatic cell population is heterogeneous. a, Summary of different co-expression patterns obtained from 53 dFISH experiments. Also refer to Supplemental Table 2. **b-d**, Confocal sections of dFISH to detect irradiation-sensitive genes (green) with *h2b* or *mcm2* (magenta). Cyan arrowheads indicate cells magnified at the far right. For (**c**), yellow arrowheads point to examples of expression in non-cycling cells.

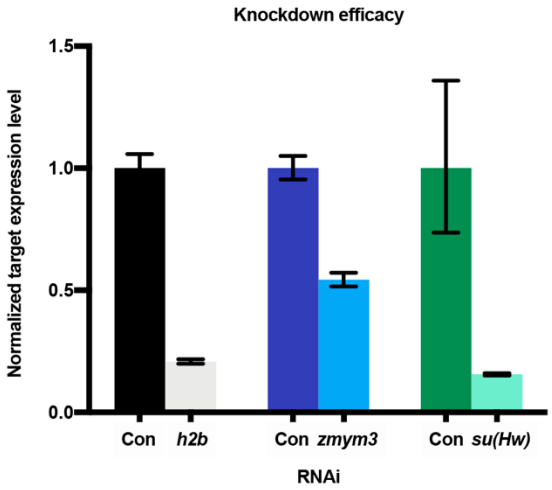

Figure 4–figure supplement 1. Validation of target gene knockdown by quantitative PCR. Knockdown of *h2b*, *zmym3*, or *su(Hw)* in whole worms observed after RNAi. Error bars: RQ min/max, N=2, n=3 each

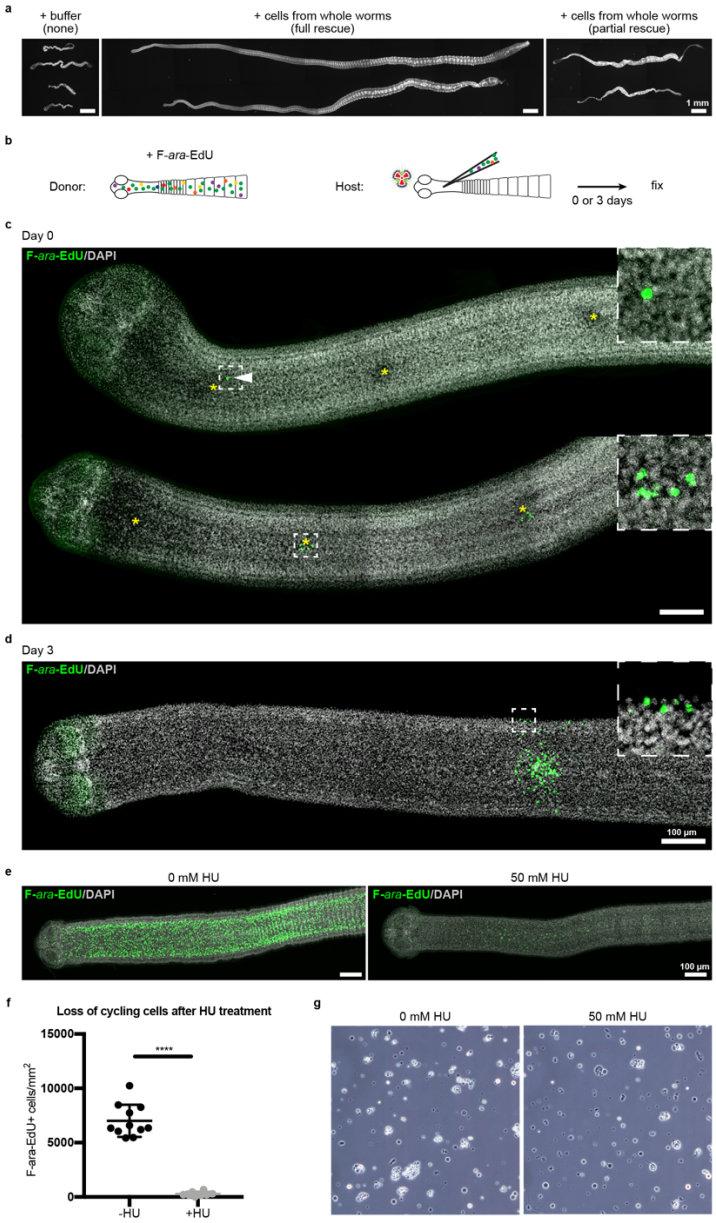

Figure 6–figure supplement 1. Stem cell activity depends on cycling cells. a, DAPI-stained worms showing phenotypes observed after attempted rescue of irradiation-induced lethality. No rescue results in degenerated worms with no proglottids, full rescue results in normal worms with multiple proglottids, and partial rescue refers to worms with visible proglottids but with defects such as contracted necks. **b**, Schematic for rescue experiment using donors with labeled cycling cells. **c-d**, Maximum-intensity projections of tile-stitched confocal sections 0 or 3 days post-transplanation according to (**b**). Injections sites marked with asterisks. White arrowhead points to a single transplanted cell. After 3 days, large colonies of F-*ara*-EdU^{+} (green) cells could be detected with some labeled cells incorporated into terminally differentiated tissues at the animal edge (inset). **e**, Maximum-intensity projections of tile-stitched confocal sections after 1 hr F-*ara*-EdU uptake (green) from control worms or worms cultured with hydroxyurea (HU) for 6 days. **f**, Quantification of cycling cells from (**e**). Error bars=SD, N=3, n=11 and 8, Student's t-test. **g**, Cell morphology with or without HU treatment prior to transplantation.

Supplemental Table 1. Irradiation-sensitive transcripts identified by RNA-seq.

Supplemental Table 2. Summary of dFISH experiments with irradiation-sensitive genes and cycling cell markers *h2b* and/or *mcm2*.

Supplemental Table 3. Anterior-enriched and anterior-depleted neck transcripts by RNA-seq.

Supplemental Table 4. Sequences and primers for all genes reported.